An Analytical Representation of Chip Area for Corner-Radiused Tools Under Both Depth-of-Cut and Feed Variations

O. Burak Ozdoganlar
Graduate Student Research Assistant

William J. Endres
Assistant Professor, Mem. ASME

Department of Mechanical Engineering and
Applied Mechanics,
University of Michigan,
Ann Arbor, MI 48109-2125

The operation of corner-radiused tools under both depth-of-cut and feed variation is a situation that occurs for many processes (e.g., straight turning, contour turning, boring, and face-milling) and under many practical conditions. A new chip-area expression is formulated by applying a rotational transformation to the chip-area geometry. Results obtained with this new representation are compared to an exact area computation algorithm based on geometric shapes. The new representation and its associated expressions are far more simple than those of the exact area representation. The errors introduced by the new representation have been analyzed and found to be very small. To increase the accuracy of the expressions for numerical applications, numerical and analytical error-compensation functions have been developed. The latter makes the expressions exact, at the expense of increased algorithmic content, whereas the former is less algorithmic with negligible errors even under extreme conditions.
[S1087-1357(00)00404-4]

1 Introduction

Since the early days of metal cutting research, researchers have observed the machining force to be proportional to the cross-sectional area of the uncut chip being removed. This *chip area* is defined as that area bounded by the tooth edge profiles corresponding to two tooth passes. The theoretical analysis of machining processes, dating back to the early 1940s or before, has considered this fact and modeled the machining force components as proportional to the chip area [1]. However, in the presence of vibration, runout or certain special cutter designs (e.g., step mill cutters), as well as contour turning applications, establishing an analytical chip-area expression is no trivial matter when working with processes used by industry, i.e., those that exhibit complex tooth forms.

The most common tooth form seen in turning, boring, and face milling processes consists of a straight major (lead) cutting edge, a straight minor (end/trail) cutting edge, and a corner (radiused) edge that connects/blends together the two straight edges. Since the presence of two straight edges (major and minor) implies that there exists a corner, and since it is the radius of the corner that is primarily responsible for the complexity of this geometry, we have termed the ensuing chip-area representation and analysis to be for *corner-radiused tools*.

1.1 Background and Motivation. A traditional graphical representation of the chip area is shown in Fig. 1, where r_ϵ is the corner radius and ψ_r is the lead angle. Shown here is the simple situation, which is often considered, where feed direction (and feed *f*) is defined to be parallel to the uncut surface and a depth direction (and depth of cut *d*) is defined to be perpendicular to the feed direction. The depth of cut is measured from the uncut surface with positive values directed into the workpiece. Since the current- and previous-pass profiles are equally spaced by a distance *f* in the feed direction, at all points down to the profile tips, they are parallel. This fact has been recognized and exploited for years to obtain the commonly seen chip area expression

$$a = fd - a_c. \tag{1}$$

Here, a_c is the area of the cusp left on the cut surface at the intersection of the current-pass and previous-pass profiles, which must be subtracted since it is excessively included in the simple product *fd*. Though the cusp area becomes negligibly small in comparison to *fd* as the depth increases, it can introduce noticeable error at high feed and low depth of cut.

The feed typically consists of the nominal feed per tooth f_t and the profile-to-profile variation in the feed direction Δf:

$$f = f_t + \Delta f. \tag{2}$$

The area model of Eqs. (1) and (2) is attractive since *fd* is a simple product involving the set depth of cut, the set feed per tooth and a well defined feed variation, while a_c is a fairly simple function of feed, corner radius and sometimes, in extreme cases, the lead and trail (end-cutting) edge angles. However, ''realities'' of machining introduce profile-to-profile variation in the depth direction as well. Depth-direction variation may come from a variety of sources, such as vibration, runout, special cutter designs, and contour turning.

Numerous investigators have addressed, to a varying degree, feed and depth variations in their modeling efforts. Feed variation can be handled in a straightforward manner (Eq. (2)) in static models, such as that of Young et al. [2]. Zhang et al. [3] developed a dynamic boring process model where the corner radius was taken to be zero, which is a good approximation when the depth of cut is substantially larger than the corner radius. DeVor et al. [4] acknowledged both radial (feed-direction) and axial (depth-direction) throw, and accounted for the former in their mechanistic force model for face milling. Enhanced dynamic models of face milling [5] and cylinder boring [6] included both tooth throw and vibration-induced variations in both directions. They made use of four geometric shapes, two of which exhibited areas that were computed through direct integration. The simulation approach of Tansel [7] used to study turning stability relies solely on numerical area integration and as such is very computationally expensive and obviously not suited to analytical methods.

Given the numerous sources of depth-direction variation and the fact that the general case of corner-radiused cutting represents

Contributed by the Manufacturing Engineering Division for publication in the JOURNAL OF MANUFACTURING SCIENCE AND ENGINEERING. Manuscript received Dec. 1997; revised Dec. 1999. Associate Technical Editor: K. Ehmann.

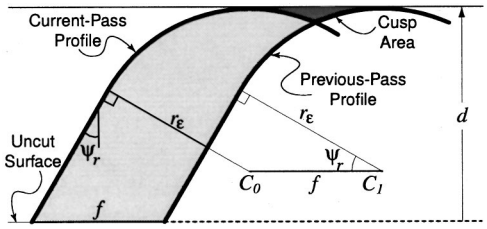

Fig. 1 Traditional simple representation of the corner-radiused chip area

many tooth geometries seen in practice, a simple analytical expression for chip area in the presence of *both* depth and feed variation has widespread use. Furthermore, the simple analytical representation presented here provides far superior computational speed as compared to the highly algorithmic and/or numerical integration-based schemes, which are employed for each tooth at each time step in time-domain simulations. This analytical representation also opens the door to accounting for depth-direction vibration in analytical machining dynamics, where one seeks analytical solutions for stability limit and vibration level.

1.2 Comparative Representations. Some of the most recent advances in characterizing the effect of depth-direction variation on chip area for corner-radiused tools include works by Endres et al. [8], Radulescu [9], and Gu [10]. A previously unpublished approach developed by Endres, which is based on geometric shapes, will be presented in the Error Analysis section, which was chosen for its simplicity and computational efficiency. The analytical representation presented and analyzed for errors in the remainder of the paper is substantially more simple from an algorithmic standpoint, exhibits negligible computational complexity, and is suitable for application in analytical machining dynamics.

Other simple approximations can be considered as alternatives to the representation presented here. Those considered here for comparison are simple products of feed and 1) the current-pass depth of cut d_0, 2) the previous-pass depth of cut d_1, and 3) the mean of the current- and previous-pass depths of cut. It will be shown that the new representation, given the end result provided here, is far superior to these three oversimplified alternatives.

1.3 The New Analytical Representation. Irrespective of the source of depth-direction variation, the variation can be identified as some Δd so that a single analysis can be conducted to cover all the aforementioned practical situations. Here, Δd is measured from the tip of the nominal profile and is positive in the direction into the workpiece so that a positive Δd increases the depth of cut. Figure 2 depicts the geometry of two tooth profiles in the presence of variations in both depth and feed (captured in f through Eq. (2)). Recognizing that the profiles are equally spaced in an ''equivalent'' feed direction, they can be considered parallel when traversed along an equivalent depth. Hence, the same simple approach of Eq. (1) may be used where f is replaced by an equivalent feed and d is replaced by an equivalent depth of cut. Indicating the equivalent variables with a star subscript, the resulting new chip area representation is

$$a = f_* d_* - a_{c*}. \tag{3}$$

This representation is basically a rotational transformation of Eq. (1).

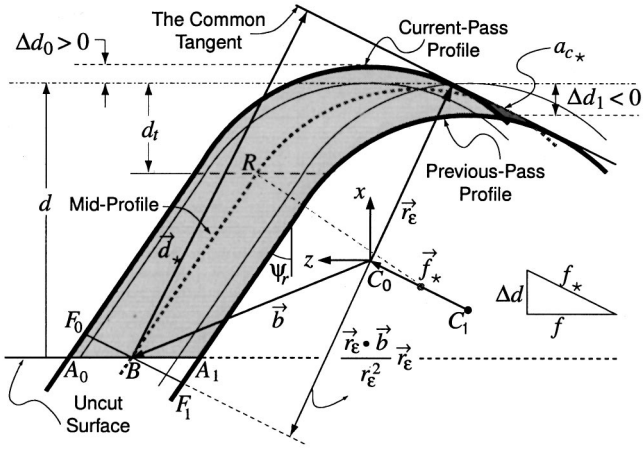

Fig. 2 Chip-area geometry with depth-direction variation Δd, where $\Delta d = \Delta d_0 - \Delta d_1$

2 Chip-Area Derivation

Derivation of the chip-area expressions requires classification of the tooth-profile pair into two cases—*small depth and large depth*—depending on the values of lead angle, corner radius, and depth of cut. The transition between the two cases occurs at a *transition* depth of cut d_t. The transition depth of cut is referenced to a (virtual) *mid-profile* that is shown in Fig. 2 as a thick dashed line between the current- and previous-pass profiles. It is centered, in the equivalent feed direction, between those two profiles. The transition depth is defined as that for which the line segment A_1A_0 passes through point R—the point on the mid-profile where the corner arc transitions into the straight lead edge. Segment A_1A_0 lies at the uncut surface and extends from the previous-pass profile to the current-pass profile. From the geometry of Fig. 2,

$$d_t = r_\epsilon(1 - \sin\psi_r) - \frac{\Delta d_0 + \Delta d_1}{2}, \tag{4}$$

where Δd_0 and Δd_1 are the variations of the current- and previous-pass depths of cut, respectively, relative to the nominal depth of cut d. Having only one condition ($d < d_t$,?) separating two cases is desirable for both analytical and numerical applications as compared to having multiple conditions with additional cases, which introduces algorithmic complexity.

2.1 Large Depth Case. The geometry for the large depth case ($d \geqslant d_t$) is illustrated in Fig. 2. In this figure, a numeric subscript on any symbol indicates that it is associated with that many tooth passes prior to the current pass ($0 \rightarrow$current, $1 \rightarrow$one previous). The equivalent feed vector, $\mathbf{f}_*$, is defined as the vector stretching from the center (C_1) of the corner arc for the previous-pass to that of the current-pass (C_0). The equivalent depth-of-cut vector is defined to be the vector perpendicular to $\mathbf{f}_*$, and stretches from point B to the *common tangent* of the two corner arcs, which is parallel to $\mathbf{f}_*$, by definition.

Defining the location of point B dictates the accuracy of the chip-area expressions since it represents the definition of the ''equivalence'' approximation. Point B identifies the intersection of the line segment A_1A_0 and the equivalent feed segment F_1F_0, the latter of which is drawn in the f_* direction such that it connects the current- and previous-pass profiles. As mentioned above, the location of A_1A_0 is fixed at the uncut surface. Hence, defining the location of F_1F_0, which must intersect A_1A_0, is analogous to locating point B. In reference to Fig. 2, the chip area representation of Eq. (3) includes the area of triangle A_0BF_0 whereas the actual chip area includes the area of triangle A_1BF_1 instead. Therefore, the location of F_1F_0 (the equivalency) should be chosen such that the areas of these two triangles are as close to equal as possible. The closer they are to equal, the better their cancellation will be, which leads to a reduced error in the equivalent representation compared to the actual/exact chip area.

In the case shown, point B falls in the middle of A_1A_0 and makes the areas of the two triangles equal. Consequently, at first

glance, locating F_1F_0 so that point B bisects A_1A_0 seems to be the ''best'' choice. However, when considering the small depth case where A_0BF_0 and A_1BF_1 are no longer triangles, and after investigating numerous possibilities, the best definition of the equivalency is that for which point B is located on the mid-profile. In this way, point B is always located at the mid-point of F_1F_0, which is equivalent to the middle of A_1A_0 for the large depth case, but not for the small depth case.

The area solution begins by setting the origin of the x-y-z Cartesian coordinate frame to be at C_0. Physically, x, y, and z label the depth-of-cut, cutting and feed directions, respectively. The vector $\mathbf{b}$ locates point B and a vector $\mathbf{r}_\epsilon$ is defined to be orthogonal to $\mathbf{f}_*$ and to stretch from C_0 to the common tangent. Given these definitions, $\mathbf{f}_*$ and $\mathbf{r}_\epsilon$ can be expressed as

$$\mathbf{f}_* = \Delta d\mathbf{i} + f\mathbf{k} \tag{5}$$

and

$$\mathbf{r}_\epsilon = \frac{r_\epsilon}{\sqrt{\Delta d^2 + f^2}}(f\mathbf{i} - \Delta d\mathbf{k}), \tag{6}$$

where $\mathbf{i}$ and $\mathbf{k}$ are the unit vectors in the x- and z-directions, respectively, and $\Delta d = \Delta d_0 - \Delta d_1$ is the total depth variation. Using vector algebra, $\mathbf{d}_*$ can be computed as

$$\mathbf{d}_* = \mathbf{r}_\epsilon - \frac{\mathbf{r}_\epsilon \cdot \mathbf{b}}{r_\epsilon^2}\mathbf{r}_\epsilon = \mathbf{r}_\epsilon\left(1 - \frac{\mathbf{r}_\epsilon \cdot \mathbf{b}}{r_\epsilon^2}\right). \tag{7}$$

Recalling that $\mathbf{d}_*$ and $\mathbf{f}_*$ are orthogonal

$$a = \|\mathbf{f}_* \times \mathbf{d}_*\| - a_{c*} = \|\mathbf{f}_*\|\|\mathbf{d}_*\| - a_{c*}, \tag{8}$$

where $\|\bullet\|$ determines the length of the vector on which it operates. From the geometry of Fig. 2, $\mathbf{b}$ can be derived as

$$\mathbf{b} = (r_\epsilon - d_0)\mathbf{i} + \left[\frac{r_\epsilon(1-\sin\psi_r)}{\cos\psi_r} - \frac{f}{2} - \left(\frac{\Delta d}{2} + d_0\right)\tan\psi_r\right]\mathbf{k},$$

where $d_0 = d + \Delta d_0$, and likewise, $d_1 = d + \Delta d_1$.

Using this expression for $\mathbf{b}$ along with Eqs. (5)–(8), the chip-area expression for the large depth case, after some manipulation, reduces to

$$a_L f d_m + r_\epsilon(f_* - f) + \Delta d(c_\psi + d_m \tan\psi_r) - a_{c*} \tag{9}$$

where

$$c_\psi = \frac{r_\epsilon(1-\sin\psi_r)}{\cos\psi_r} \tag{10}$$

and $d_m = \frac{1}{2}(d_0 + d_1)$ is the mean depth of cut.

In summary, use of the definitions of $\mathbf{f}_*$ and $\mathbf{r}_\epsilon$ are given in Eq. (5) and Eq. (6), respectively, leads to the derivation of $\mathbf{d}_*$, resulting in Eq. (7). Then, deriving the *case-specific* $\mathbf{b}$ from the profile-pair geometry, substituting it into the $\mathbf{d}_*$ expression, and substituting $\mathbf{d}_*$ into Eq. (8) leads to the area expression of Eq. (9).

2.2 Small Depth Case. The same derivation method as above applies for the small depth case, which is shown in Fig. 3. The difference lies only in computing the case-specific vector $\mathbf{b}$. From the geometry in Fig. 3,

$$\mathbf{b} = (r_\epsilon = d_0)\mathbf{i} + \left(\sqrt{d_m(2r_\epsilon - d_m)} - \frac{f}{2}\right)\mathbf{k}.$$

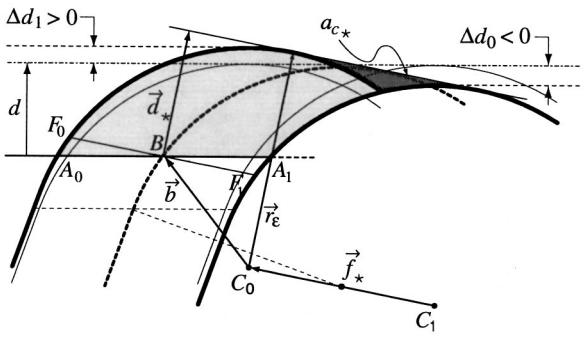

Fig. 3 Small depth geometry

Using this $\mathbf{b}$ together with Eqs. (5)–(8), the chip-area expression for the small depth case eventually reduces to

$$a_s = f d_m + r_\epsilon(f_* - f) + \Delta d\sqrt{d_m(2r_\epsilon - d_m)} - a_{c*}. \tag{11}$$

2.3 Cusp Area Expression. The expression for the cusp area a_c is well known to be

$$a_c = f r_\epsilon - \frac{f}{2}\sqrt{r_\epsilon^2 - \frac{f^2}{4}} - r_\epsilon^2 \arcsin\left(\frac{f}{2r_\epsilon}\right). \tag{12}$$

Comparing the cusp region of Fig. 1, viewed in the $f-d$ coordinates, to that of Figs. 2 and 3, viewed in the f_*-d_* coordinates, clearly indicates an equivalent shape. Thus, the equivalent cusp area can be established by substituting f_* for f in Eq. (12).

The equivalent cusp area expression given above is valid when the two profiles intersect on their corner arcs. However, for extreme values of depth variation and feed, the intersection can be that of the current-pass trail (end-cutting) edge and the previous-pass corner arc, the current-pass corner arc and the previous-pass lead edge or the current-pass trail edge and the previous-pass lead edge. Investigation of these less common cases is simply an algebraic exercise; hence, it is left as an implementation exercise.

2.4 Validity Constraints. Though chip-area expressions may produce negative values, only non-negative values make physical sense. The chip area becomes zero when the current-pass profile completely disengages the workpiece. In practice, this occurs in the presence of large tooth throws and/or when the chatter condition is reached due to excessive vibrations. For the case when only a feed direction variation is considered, zero chip area translates into either the feed or the depth being zero. However, when both the depth and feed variations are non-zero, the tooth engagement ceases causing the chip area to become zero for any configuration where the current-pass profile is located ''inside'' the previous-pass profile. This physical limitation can be expressed as

$$f + \Delta d\tan\psi_r > 0 \quad \text{and} \quad f - \frac{\Delta d}{\tan\kappa_{r'}} > 0,$$

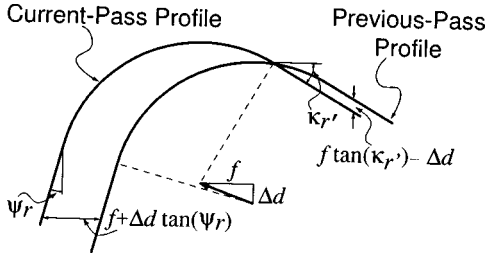

Fig. 4 Finite-positive validity constraints

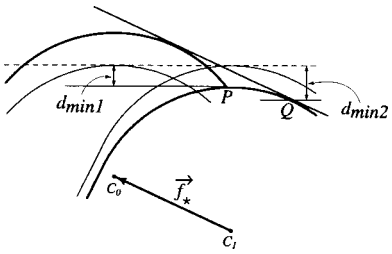

Fig. 5 Minimum depth for $\Delta d>0$

where κ_r, is the trail (end cutting) edge angle. Figure 4 shows the dimensions corresponding to the left-hand sides of these constraints.

The first condition assures tooth engagement so that the chip area is positive. The second condition assures that the chip area is finite, i.e., a bounded region. The fact that κ_r, always assumes a value between 0 deg and 90 deg is considered when writing the second condition. Should tan κ_r, be zero, this condition becomes $f>\Delta d\cdot\infty$. This implies that when $\Delta d\geqslant 0$ no acceptable finite value of f will result in the chip-area being bounded. On the other hand, a finite chip area would exist for all $\Delta d<0$. In other words, when the second condition is not met, meaning the previous-pass profile does not intersect the current-pass profile to form/close the chip area, there must exist, in practice, some earlier tooth profile for which the condition is satisfied. This is an implementation issue that exists for any chip-area computation algorithm.

In addition to satisfying the above constraints, there exists a nominal depth constraint for the new chip-area representation. It is imposed so that the cusp area is always completely below the nominal depth of cut. Figures 5 and 6 illustrate the three candidate minimum depth values. The first two are of interest when $\Delta d>0$, with the first arising from the intersection of the previous- and current-pass corner arcs at point P. From the geometry in the figure, the first candidate value can be written as

$$d_{min1}=r_\epsilon\frac{f}{f_*}\sqrt{r_\epsilon^2-\frac{f_*^2}{4}}-\frac{1}{2}(\Delta d_0+\Delta d_1).$$

Defining point Q to be the intersection of the common tangent and the previous-pass corner arc, the second candidate value is written as

$$d_{\min 2}=r_\epsilon-\frac{f}{f_*}-\Delta d_1.$$

Consequently, when $\Delta d>0$, the minimum depth value is the larger of the two candidate values, i.e., $\max[d_{min1},d_{min2}]$.

Figure 6 shows the case for $\Delta d<0$. Here, a minimum equivalent depth, d_{*min}, can be defined as the distance between the common tangent and a line that is parallel to the common tangent and passes through point P. Thus, the minimum depth for $\Delta d<0$ can be expressed as

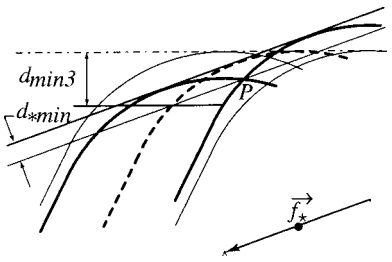

Fig. 6 Minimum depth for $\Delta d<0$

$$d_{min3}=r_\epsilon-\frac{f}{f_*}\sqrt{r_\epsilon^2-\frac{f_*^2}{4}}-\Delta d_0.$$

To minimize the algorithmic complexity (number of intermediate conditions and corresponding cases), we wish to avoid different expressions for $\Delta d<0$ and $\Delta d>0$; hence, a single minimum depth is computed as

$$d_{min}=\max[d_{min1},d_{min2},d_{min3}].$$

Of course, at depths below d_{min}, the chip area is simply that of an arc segment, the exact value of which is easily computed if desired.

3 Error Analysis

Since the presented chip area is an approximation, it must be analyzed in terms of the errors it introduces. Comparison is made to the exact area and to the three alternate, highly simplified expressions mentioned in the introduction.

When conducting the error analysis and later formulating a compensation term it is advantageous to remove the corner radius as a variable by nondimensionalizing depths ($d,d_*,\Delta d$, etc.) and feeds (f and f_*) by r_ϵ. Uppercase symbols to follow represent nondimensional variations of their respective lowercase symbols, that is, that lowercase variable divided by r_ϵ for all variables except A and A_{c*}, which are their respective variable divided by r_ϵ^2. Note that all the above results can be nondimensionalized as well.

3.1 Comparison to Exact and Simplified Representations. A method to compute the exact chip area, in the presence of depth and feed variations, has been developed by Endres based on addition and subtraction of geometric shapes. Figure 7 illustrates the geometric shapes for the large depth case. Subtracting the cross-hatched area, a circular segment, from the shaded area composed of three triangles and a circular segment, the exact area is obtained. This exact result is very computationally complex and fairly algorithmic since it includes many cases with several conditions, and requires the coordinates of each of the five points in Fig. 7 to be computed. Such complexity is typical of and in some cases worse in the other methods cited earlier [8–10].

In the ensuing error analysis, ranges of variables have been chosen to encompass some of the most extreme conditions encountered in practice: $-0.6\leqslant\Delta D\leqslant 0.6$, $0.15\leqslant F\leqslant 0.9$, and -45 deg$\leqslant\psi_r\leqslant 30$ deg. The analysis is performed considering ΔD to be evenly distributed about the nominal profiles, i.e., $\Delta D_0=-\Delta D_1$. If ΔD is not evenly distributed about the nominal depth, one would simply observe the same errors, only shifted along the depth axis.

For a given $|\Delta D|$, the percent errors for $\Delta D<0$ are much larger in magnitude than for $\Delta D>0$. This is a result of the exact area, *relative to which the percent error is computed*, being much

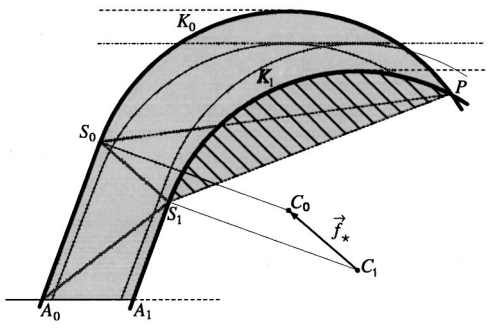

Fig. 7 Exact area calculation using geometric shapes

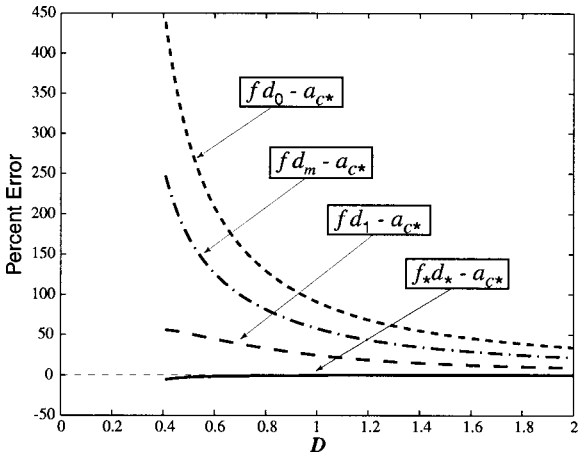

Fig. 8 Comparison of the percent errors with those of the alternate expressions

smaller when $\Delta D<0$ than when $\Delta D>0$. Additionally, all errors approach zero as D increases, and more specifically, becomes zero for

$$D \geqslant D_z = \max[(1-\sin\psi_r - \Delta D_0),\quad (1-\sin\psi_r - \Delta D_1)]. \tag{13}$$

As a consequence of the exact area getting larger with increasing feed as well, the percent errors decrease, in the absolute value, with increasing feed.

Figure 8 shows a comparison, in terms of percent errors, to the three highly simplified chip-area expressions noted in the introduction. Clearly, the new chip-area representation results in much smaller percent errors. In addition, while the percent error of the new expression becomes zero for the large-depth case, the alternative expressions still exhibit large errors. The conditions used to generate this comparison yield some of the smallest errors in the alternate expressions that were observed across all conditions considered here.

3.2 Error Compensation. For use in analytical stability solutions, since infinitesimal displacements about equilibrium are considered ($\Delta d \sim 0$), the error is virtually zero. Compensating for the error, however, is of interest for implementation in numerical time-domain simulations where the new representation can significantly enhance computational efficiency.

3.2.1 Analytical Error Compensation. The source of errors can be clearly seen in Fig. 9. The actual chip area is $\mathcal{A}(A_0PA_1)$, whereas the chip area computed via the above representation is $\mathcal{A}(F_0PA_0)$. Therefore, the chip-area expression presented here includes the area $\mathcal{A}(BA_1F_1)$ in place of $\mathcal{A}(A_0F_0B)$. Due to the way the point B is chosen, the two triangular areas $\mathcal{A}(S_0F_0B)$ and $\mathcal{A}(BS_1F_1)$ are identical (which is precisely why the chip area

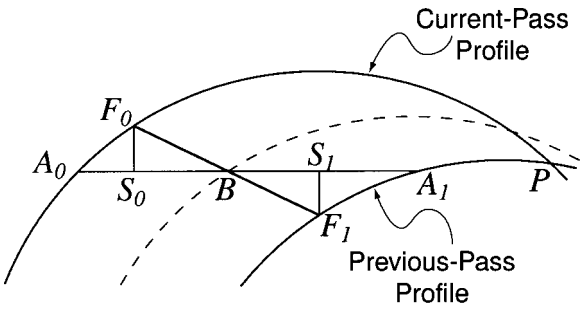

Fig. 9 Source of errors

expression is exact for large depths). Hence, the difference between the areas, $\mathcal{A}(A_0F_0S_0)$ and $\mathcal{A}(F_1S_1A_1)$ would be the error associated with the chip-area expressions. This area can be calculated exactly and directly through the geometry of Fig. 9. Their shapes change based on the depth of cut and the sign of Δd, which should be considered when calculating these areas. The compensation areas for positive lead angles are

$$a_{aec1} = \frac{r_\epsilon^2}{2}(\theta_1-\theta_0) - \Delta d s_m + \frac{1}{2}(s_1 l_1 - s_0 l_0) \quad \text{for} \quad d \leqslant d_t - \frac{|\Delta d|}{2},$$

$$a_{aec2} = \frac{l_1 r_\epsilon}{\cos\psi_r} - \Delta d s_m + \frac{r_\epsilon^2}{2}(\psi_r - \tan\psi_r - \theta_0) + \frac{1}{2}(-l_0 s_0 - l_1^2 \tan\psi_r) \quad \text{for} \quad d_t \geqslant d > d_t - \frac{|\Delta d|}{2} \quad \text{and} \quad \Delta d<0,$$

$$a_{aec3} = -\frac{l_0 r_\epsilon}{\cos\psi_r} - \Delta d s_m + \frac{r_\epsilon^2}{2}(-\psi_r + \tan\psi_r + \theta_1) + \frac{1}{2}(l_1 s_1 - l_0^2 \tan\psi_r) \quad \text{for} \quad d_t \geqslant d > d_t - \frac{|\Delta d|}{2} \quad \text{and} \quad \Delta d>0,$$

$$a_{aec4} = \frac{l_0 r_\epsilon}{\cos\psi_r} + \Delta d l_m \tan\psi_r + \frac{r_\epsilon^2}{2}(\psi_r - \tan\psi_r + \theta_0) + \frac{1}{2}(-l_0 s_0 - l_1^2 \tan\psi_r) \quad \text{for} \quad d_t + \frac{|\Delta d|}{2} \geqslant d > d_t \quad \text{and} \quad \Delta d<0,$$

$$a_{aec5} = -\frac{l_1 r_\epsilon}{\cos\psi_r} + \Delta d l_m \tan\psi_r + \frac{r_\epsilon^2}{2}(-\psi_r + \tan\psi_r + \theta_1) + \frac{1}{2}(l_1 s_1 - l_0^2 \tan\psi_r) \quad \text{for} \quad d_t + \frac{|\Delta d|}{2} \geqslant d > d_t \quad \text{and} \quad \Delta d>0,$$

where

$$l_\bullet = r_\epsilon - d_\bullet, \quad s_\bullet = \sqrt{r_\epsilon^2 - d_\bullet} \quad \text{and} \quad \theta_\bullet = \arcsin\left(\frac{l_\bullet}{r_\epsilon}\right).$$

Adding to the appropriate (small or large depth) chip area expression given in Eqs. (9) and (11), the compensation term associated with the condition at hand makes the resulting expressions exact. Although more involved and algorithmic, analytical error compensation terms for negative lead angles can be established in the same way.

3.2.2 Numerical Error Compensation. Although the analytical error compensation introduced above makes the chip-area expressions exact, it increases the algorithmic content of the expressions. A numerical and less algorithmic error compensation term can be derived as well with the intent being to achieve a near-exact result with little additional algorithmic complexity. Its development is based on the trends of the non-dimensional errors

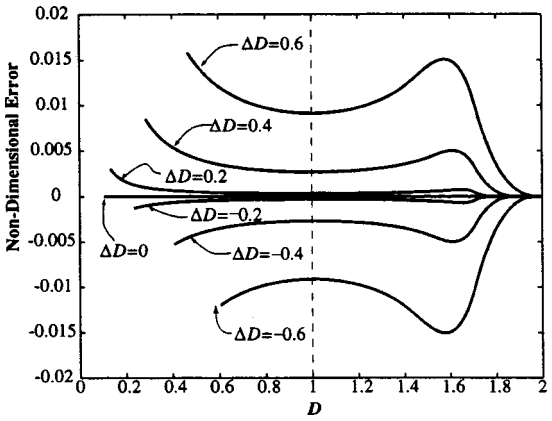

Fig. 10 Non-dimensional errors for $\psi r = -45°$

with respect to ΔD (Fig. 10) and lead angle (Fig. 11). As seen in Fig. 10, the trends at depths of cut well below the transition depth (D_t) are even functions of normalized depth, D, being symmetric about $D=1$ and mirrored about an error value of zero for positive and negative levels of each $|\Delta D|$. Figure 11 shows that the lead angle affects the depth of cut at which the decaying departure occurs from the even, symmetric curves shown in Fig. 10 for the extreme lead angle of -45 deg. These observations lead to a two-part error compensation function that provides a superposition of these two trends. The resulting error compensation term is $A_{nec}=A_{nec1}+A_{nec2}$, where A_{nec1} represents the symmetric portion of the error curves and A_{nec2} represents the ψ_r-dependent departures from the symmetric curves. The first term has the form

$$A_{nec1}=\begin{cases} b_2[1+b_1(D-1)^4]\Delta D^3, & \text{for} \quad D<D_t \\ 0 & \text{for} \quad D\geqslant D_t \end{cases},$$

where $b_1=-7.524$ and $b_2=-4.421\times10^{-2}$. The second term has the form

$$A_{nec2}=\frac{-c_1c_2\,\mathrm{sgn}(\Delta D(D-D_t))}{[\sqrt{c_1}+c_1\sqrt{c_2}|D-D_t|]^2},$$

where $c_1=2\times10^5$ and $c_2=c_{20}+c_{22}\psi_r^2+c_{24}\psi_r^4$. Here, ψ_r is measured in radians and

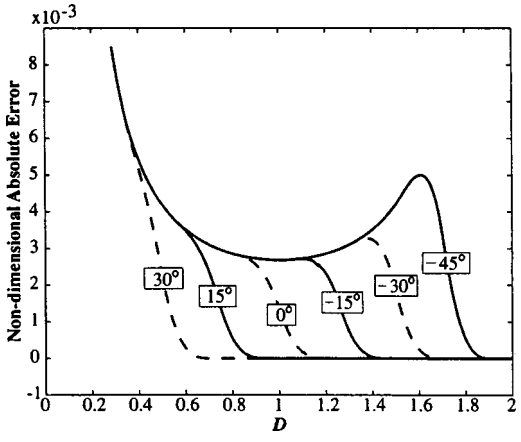

Fig. 11 Effect of the lead angle (labeled $-45°$ to $30°$) on absolute error

$$c_{20}=4.34\times10^{-3}\Delta D^2+2.27\times10^{-2}\Delta D^4$$

$$c_{22}=1.51\times10^{-3}\Delta D^2+2.07\times10^{-2}\Delta D^4$$

$$c_{24}=2.13\times10^{-3}\Delta D^2+7.78\times10^{-2}\Delta D^4.$$

Including the error compensation terms reduces the errors substantially. For the case of $\Delta D=-0.4$ and $\psi_r=0$ deg, which exhibits some of the worst errors across all ΔD that were considered, the maximum absolute value of the percent error for this case is decreased from 28 percent to 1.8 percent for $F=0.15$ and from 24 percent to 1.2 percent for $F=0.3$. Since the data used to formulate this numerical error compensation expression was based on $\Delta D_0=-\Delta D_1$, the mean nondimensionalized depth ($D_m=d_m/r_\epsilon$) should be used for D in these expressions.

4 Summary and Conclusions

A new analytical chip-area representation for corner-radiused tools under both depth-of-cut and feed variation was presented. Based on this representation, chip-area expressions were derived for ''small'' and ''large'' depth cases using a vectorial approach. The resulting errors were analyzed across wide ranges of conditions within the validity constraints. The percent errors of the new representation are far better than those of three alternate representations introduced for comparison purposes. Analytical error compensation functions have been derived, addition of which makes the chip area expressions exact, but at the expense of increased algorithmic content. An alternative, less algorithmic, numerical compensation function was also derived, which reduces the errors to near zero for all conditions surveyed without introducing any significant complexity in the computations or algorithms.

Acknowledgments

The authors are pleased to acknowledge the financial support of the Engineering Research Center for Reconfigurable Machining Systems (NSF grant EEC-9529125), and the assistance from the members of the ERC (both industry and academia). The authors also acknowledge the assistance of graduate student Gustavo A. Delfino for his assistance at the initial stage when this was studied as a class project, and of graduate student Scott G. Taylor for his assistance in improving the numerical error compensation.

References

[1] Merchant, M. E., 1944, ''Basic Mechanics of Metal Cutting Process,'' ASME J. Appl. Mech., **66**, pp. A168–A175.
[2] Young, H. T., Mathew, P., and Oxley, P. L. B., 1989, ''Allowing for Nose Radius Effects in Prediction Chip Flow Direction and Cutting Forces in Bar Tuning,'' Inst. Mech. Eng., Part C, **201** (C3), pp. 42–49.
[3] Zhang, G. M., and Kapoor, S. G., 1987, ''Dynamic Modeling and Analysis of the Boring Machining System,'' ASME J. Eng. Ind., **109**, pp. 219–226.
[4] DeVor, R. E., Kapoor, S. G., Fu, H. J., and Subbarao, P. C., 1983, ''Effect of Variable Chip Load on Machining Performance in Face Milling,'' NAMRI/SME, **11**, pp. 348–355.
[5] Subramani, G., Kapoor, S. G., DeVor, R. E., and Hayashida, R., 1987, ''An Enhanced Model for the Simulation of Face Milling Operations,'' *Proceedings, 2nd International Conference on Computer-Aided Production Engineering*, pp. 42–49.
[6] Subramani, G., Suvada, R., Kapoor, S. G., DeVor, R. E., and Meingast, W., 1987, ''A Model for the Prediction of Force System for Cylinder Boring Process,'' NAMRI/SME, **15**, pp. 439–446.
[7] Tansel, I. N., 1993, ''A Unified Transfer Function (UTF) Approach for the Modeling and Stability Analysis of Long Slender Bars in 3-D Turning Operations,'' ASME J. Eng. Ind., **115**, pp. 193–204.
[8] Endres, W. J., Sutherland, J. W., DeVor, R. E., and Kapoor, S. G., 1990, ''A Dynamic Model of the Cutting Force System in the Turning Process,'' *ASME Symposium on Monitoring and Control for Manufacturing Processes*, Vol. PED **44**, pp. 193–212.
[9] Radulescu, R. C., 1993, ''A General Cutting Process Model for High-Speed Machining: Dynamics and Thermal Considerations,'' Ph.D. thesis, University of Illinois at Urbana-Champaign, Urbana, IL.
[10] Gu, F., 1994, ''Prediction of Cutting Forces and Surface Errors in Face Milling with Generalized Cutter and Workpiece Geometry,'' Ph.D. thesis, University of Illinois at Urbana-Champaign, Urbana.